

Autonomous Vehicle Control in Multi-Class Traffic Flow: Preliminary Results from Microscopic Delayed ODE Models

Zheng Chen¹, Xiaoqian Gong², Lin Mu³

¹University of Massachusetts Dartmouth, USA

²Amherst College, USA

³University of Georgia, USA

1. Introduction

Traffic congestion remains a critical challenge in urban transportation systems. Our preliminary investigations focus on the impact of autonomous vehicles (AVs) on traffic dynamics using a microscopic ODE model with delay of a ring road with stop-and-go waves. We have implemented prototype simulations incorporating a small fraction of controllable AVs and tested simple feedback control strategies. Initial results indicate that even a limited number of AVs can significantly reduce fuel consumption and mitigate traffic instabilities, demonstrating the potential for optimal control to improve overall traffic flow.

2. Model and Methods

2.1. Microscopic ODE Model for a Ring Road with Stop-and-Go Wave

We consider a ring road with N human-driven vehicles and M autonomous vehicle, where human-driven vehicles follow a standard car-following ODE model, and AVs are equipped with controllable acceleration inputs. Let $I_a \subset \{1, \dots, N+M\}$ and $I_h = \{1, \dots, N+M\} \setminus I_a$ be the set of the indices of autonomous and human-driven vehicles, respectively. Notice that $|I_a| = M$ and $|I_h| = N$. The model for vehicle $i \in \{1, \dots, N+M\}$ includes its position $\mathbf{x}_i(t)$ and velocity $\mathbf{v}_i(t)$. The equations are described as below,

$$\begin{aligned}\dot{\mathbf{x}}_i(t) &= \mathbf{v}_i(t), \\ \dot{\mathbf{v}}_i(t) &= \alpha [V(\mathbf{h}_{\tau,i}(t)) - \mathbf{v}_i(t)] + \beta \left[\frac{\mathbf{v}_{i-1}(t-\tau) - \mathbf{v}_i(t)}{\mathbf{h}_{\tau,i}(t)^2} \right], \\ \dot{\mathbf{v}}_i(t) &= \alpha_{av} [V_{av}(\mathbf{h}_i(t)) - \mathbf{v}_i(t)] + \beta_{av} \left[\frac{\mathbf{v}_{i-1}(t) - \mathbf{v}_i(t)}{\mathbf{h}_i(t)^2} \right],\end{aligned}$$

where

- $\tau > 0$ is the time delay due to the human driver's reaction time.
- $\mathbf{x}_i(t)$ is the position of vehicle i at time t .
- $\mathbf{h}_{\tau,i}(t) = \mathbf{x}_{i-1}(t-\tau) - \mathbf{x}_i(t) - l$ and $\mathbf{h}_i(t) = \mathbf{x}_{i-1}(t) - \mathbf{x}_i(t) - l$ denote the delayed and actual spacing headways of vehicle i at time t , respectively. For vehicle $N+M$, the leading vehicle is vehicle 1 due to the periodic boundary conditions and $\mathbf{h}_{N+M}(t, \tau) = \mathbf{x}_1(t-\tau) - \mathbf{x}_{N+M}(t) + L$. Here L denote the length for the ring road.
- $\mathbf{v}_i(t)$ is the velocity of vehicle i at time t . V is the optimal velocity function, which dictates the ideal speed for a driver given the distance to the vehicle ahead. A common form [1, 2] is:

$$V(h) = v_{\max} \left[\tanh \left(\frac{h - h_{\text{safe}}}{h_{\text{free}}} \right) + \tanh \left(\frac{h_{\text{safe}}}{h_{\text{free}}} \right) \right] \quad (1)$$

Here, v_{\max} is the maximum speed, h_{safe} is the safe distance, and h_{free} is a parameter that controls how quickly the driver adjusts to the optimal speed.

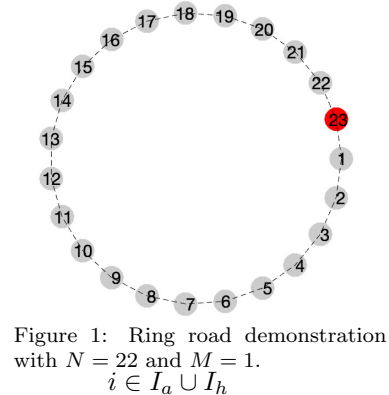


Figure 1: Ring road demonstration with $N = 22$ and $M = 1$.
 $i \in I_a \cup I_h$

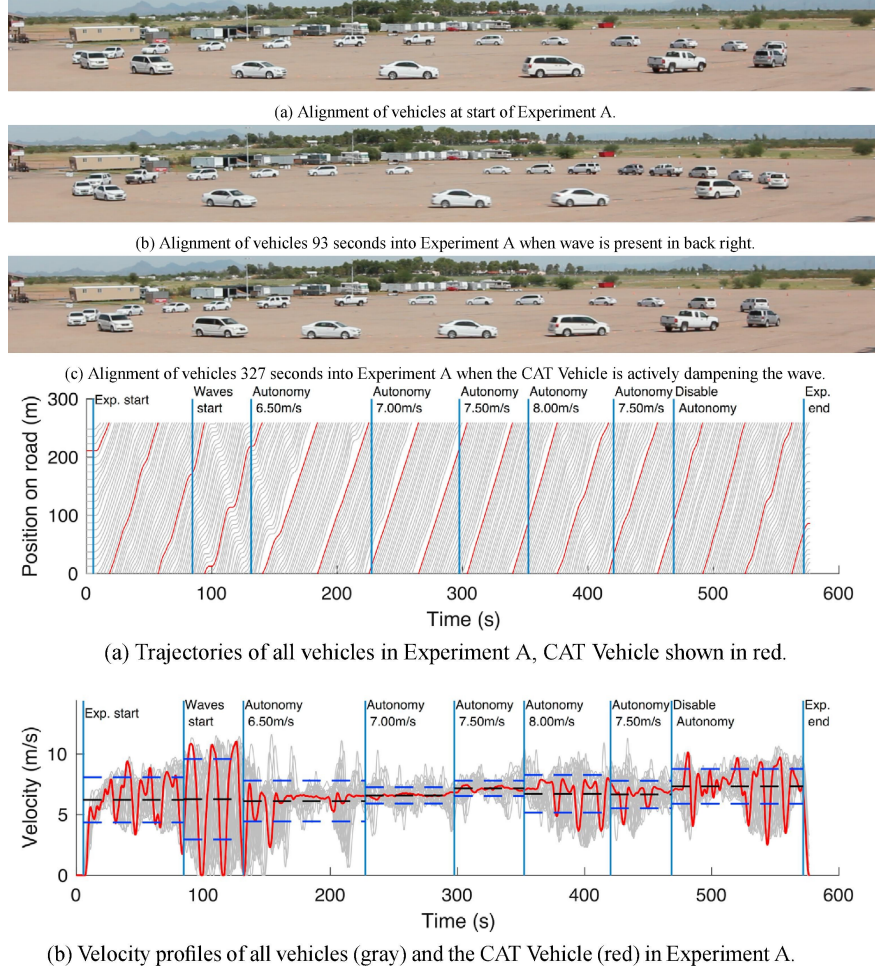
$i \in I_h$,

$i \in I_a$,

- α is the sensitivity parameter, representing how quickly a driver adjusts their speed to match the optimal velocity, while β governs the response to the relative velocity with the vehicle ahead.

2.2. Physical Experiments

Our study of microscopic ODE models for ring-road traffic with stop-and-go waves is motivated by and builds upon previous experimental observations. In particular, the field experiments conducted by Stern et al. [3] demonstrated that a single well-controlled autonomous vehicle can significantly dissipate stop-and-go waves in a circular track with human-driven vehicles. These experiments provide critical empirical evidence of the potential for AV control to stabilize traffic flow and reduce fuel consumption, which informs both the design and validation of our computational models.



Horizontal blue dashed lines are one standard deviation above and below the mean speed of traffic in the interval.

Figure 2: Results from [3].

2.3. Numerical Results

Simulation Set Up: We choose the following parameter values for testing:

- $N = 23/22, M = 0/1, L = 260, \tau = 0.2, \alpha = 0.5, v_{\max} = 11, \beta = 5, h_{\text{safe}} = 5, h_{\text{free}} = 10$
- Initial conditions are chosen such that

- $\mathbf{x}_i(0) = \frac{L}{N}(0 : N)$ - evenly space all vehicle on the ring
- $\mathbf{v}_i(0) = 0$ ($i > 1$) - initialize all vehicles except the first vehicle with a zero initial velocity; we assume a perturbed velocity for the first vehicle, and let $\mathbf{v}_1(0) = 5$.

- The following three cases have been considered
 - Case 1. 23 human-driven vehicles
 - Case 2. 22 human-driven vehicles and 1 autonomous vehicle
 - Case 3. 21 human-driven vehicles and 2 autonomous vehicles
- When the autonomous vehicle has been activated, we set $\alpha_{\text{av}} = 0.5$, $\beta_{\text{av}} = 5$ and tune the values in v_{av} in the optimal velocity as shown below

$$V_{\text{av}}(h) = v_{\text{av}} \left[\tanh\left(\frac{h - h_{\text{safe}}}{h_{\text{free}}}\right) + \tanh\left(\frac{h_{\text{safe}}}{h_{\text{free}}}\right) \right]. \quad (2)$$

- We employ different vehicle lengths as below,

Car Index	1	2	3	4	5	6	7	8	9	10	11
$l(\text{m})$	5.22	5.15	4.86	4.87	5.15	5.15	4.86	4.92	5.09	4.86	4.86
Car Index	12	13	14	15	16	17	18	19	20	21	22
$l(\text{m})$	5.69	5.21	5.15	4.87	5.15	4.86	4.87	5.15	5.70	4.44	5.15

Table 1: length of vehicles

- We assume the length for Car #23 is 5(m).

Case 1. We first perform the simulation for 23 HVs. The results are shown in Figure 3. As we observed from this figure, the period stop-and-wave forms around time = 100. The numerical results confirm the presence of a stop-and-go wave throughout the simulation. As shown in this figure, the velocity profile clearly exhibits alternating phases of acceleration and deceleration, indicating the persistence of the stop-and-go pattern. Despite progressing toward a steady state, the system continues to oscillate, and the velocity remains unstable. This instability is further supported by variations in headway and non-zero maximum acceleration values. Additionally, wave-back propagation observed in the simulation aligns with typical characteristics of stop-and-go traffic behavior. The introduction of an energy-based metric ($\max(a, 0)^2$) focusing on positive accelerations further highlights the dynamic fluctuations in vehicle behavior. Overall, these results validate the emergence and persistence of stop-and-go waves in the simulated traffic flow. It is also noted that, in the steady-state numerical solution, the energy cost is always greater than zero. Furthermore, as shown in the position plot in Figure 4, several snapshot positions are presented to further illustrate the traffic jam and the backward propagation of the wave.

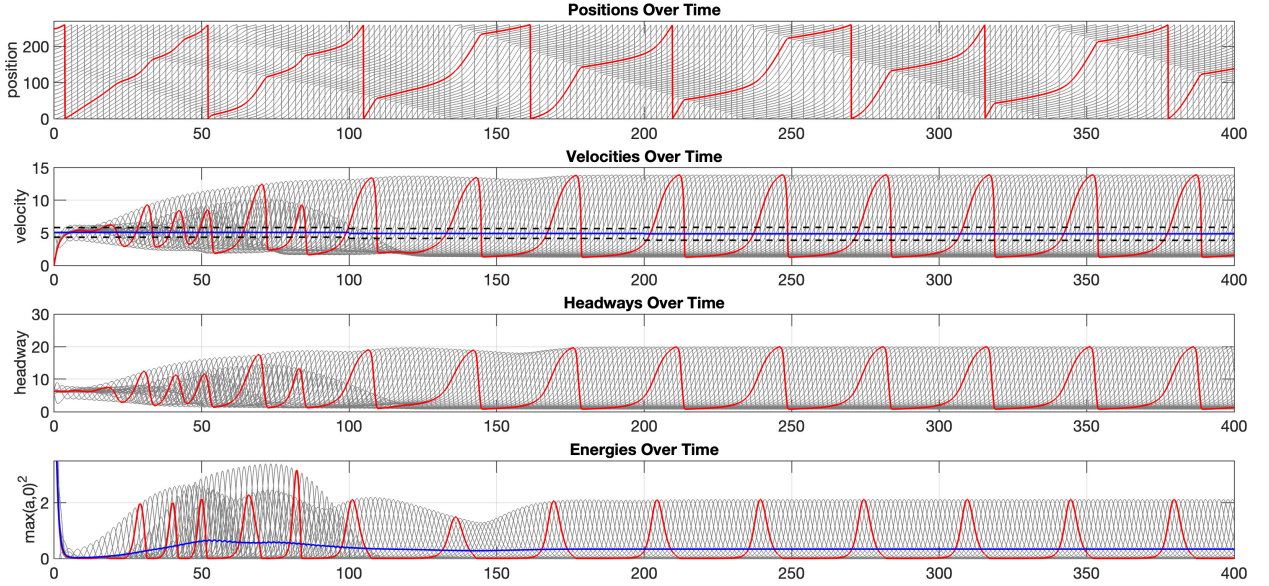


Figure 3: Case 1: Illustration of 23 HV simulation. The red curve plots the data for Car #23. Blue curves plot the mean velocity over each time intervals with length 100 and the average $\max(a, 0)^2$. The blue dotted curves plot the mean velocity \pm derivation.

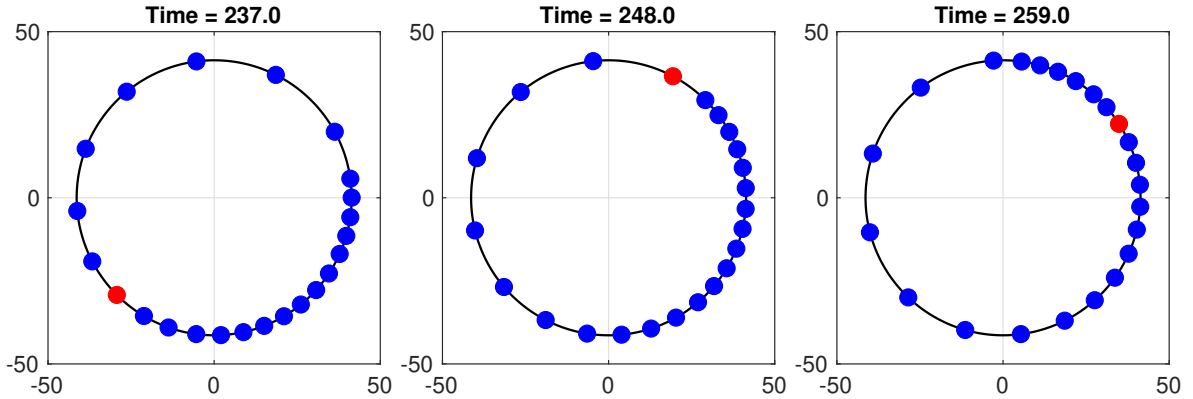


Figure 4: Case 1: Snapshot plots on various time.

Case 2. In this case, the autonomous vehicle (AV) is activated at $t = 200$ s, and the control parameter v_{av} in Equation (2) is applied for a duration of 100 seconds. Figure 5 presents system performance at 100-second intervals. Notably, the position plots demonstrate that for $v_{av} = 3, 3.5, 4$, the traffic jam is significantly mitigated, as indicated by the nearly linear vehicle trajectories compared to the pre-activation phase ($t < 200$ s). Although the system response varies with different v_{av} values, all tested cases show improved behavior relative to the human-driven baseline. Furthermore, the velocity plots in the interval $t = [1000, 1100]$ s exhibit near-constant profiles, suggesting that appropriately selecting v_{av} can lead to a stable steady-state velocity. The corresponding headway plots indicate that the AV maintains a longer following distance, effectively acting as a damping agent and contributing to smoother traffic flow during the same time period. Finally, the energy consumption, measured by the quantity $\max(a, 0)^2$, is remarkably low for $v_{av} = 3$ within $t = [1000, 1100]$ s, marking it as the most energy-efficient setting in this test. These results outperform those observed in Case 1 and highlight the importance of optimizing the AV control

parameter to enhance overall traffic stability and efficiency. Figures 6–7 present several snapshot results that confirm the improved headways and overall traffic conditions.

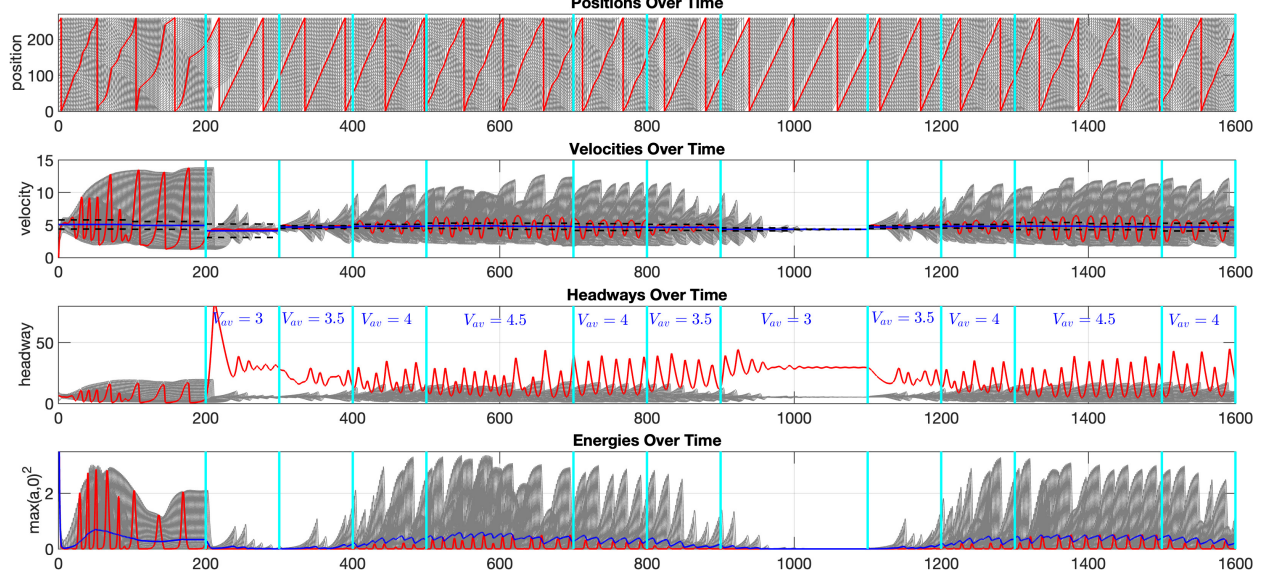


Figure 5: Case2: Illustration of 22 HV + 1AV simulation. The red curve plots the data for AV Car #23. Blue curves plot the mean velocity over each time intervals with length 100 and the average $\max(a, 0)^2$. The blue dotted curves plot the mean velocity \pm derivation.

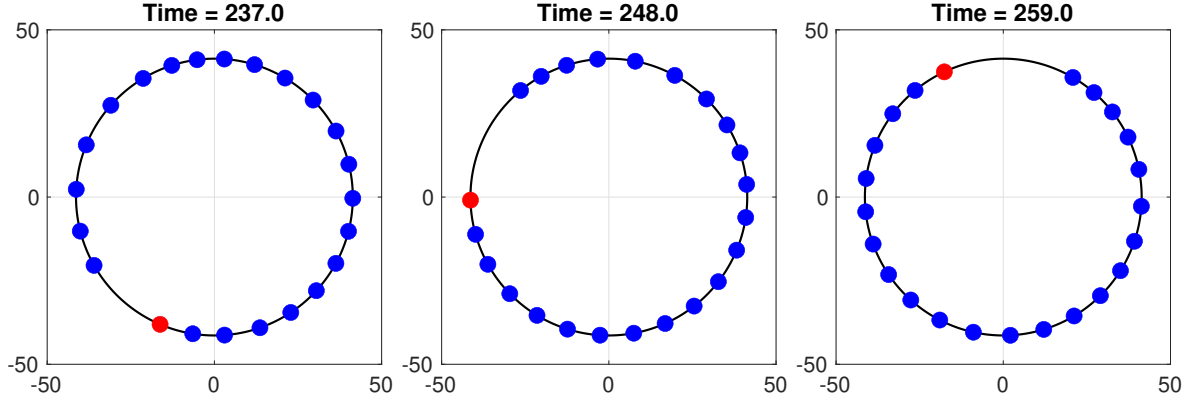


Figure 6: Case 2: Snapshot Plots

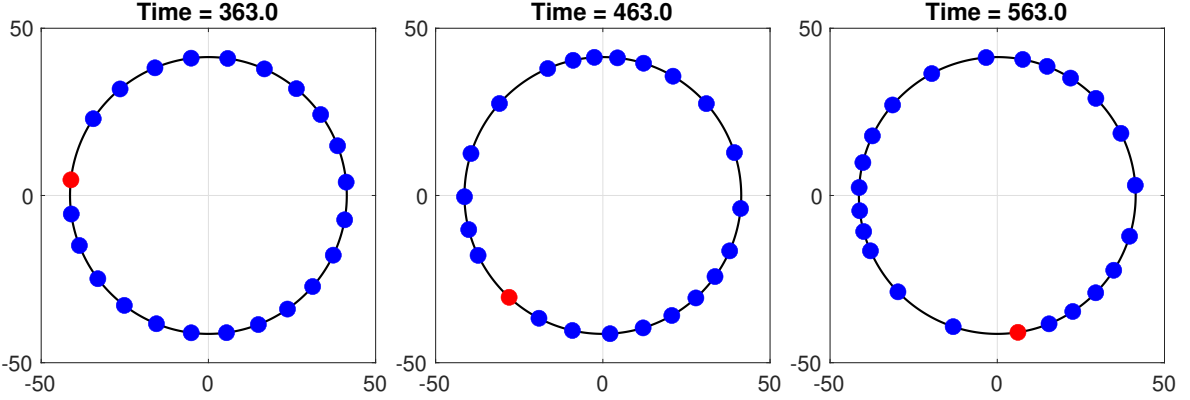


Figure 7: Case 2: Snapshot Plots

Case 3. In this case, we activate two AVs—Car #23 and Car #11—starting at time $t = 200$ s. The v_{av} parameters are tuned for both AVs, and for simplicity, identical parameter values are applied. Figure 8 presents the system performance in 100-second intervals. Compared to Case 2, traffic conditions show further improvement; for instance, the constant velocity pattern persists over a longer period within the [900, 1100] second interval. Energy costs are also further reduced. Additionally, the velocity and headway plots for Car #23 and Car #11 coincide over several time intervals, indicating stable and consistent behavior. Once again, the snapshot plots in Figures 9–10 highlight the benefits of deploying AVs in traffic jam scenarios.

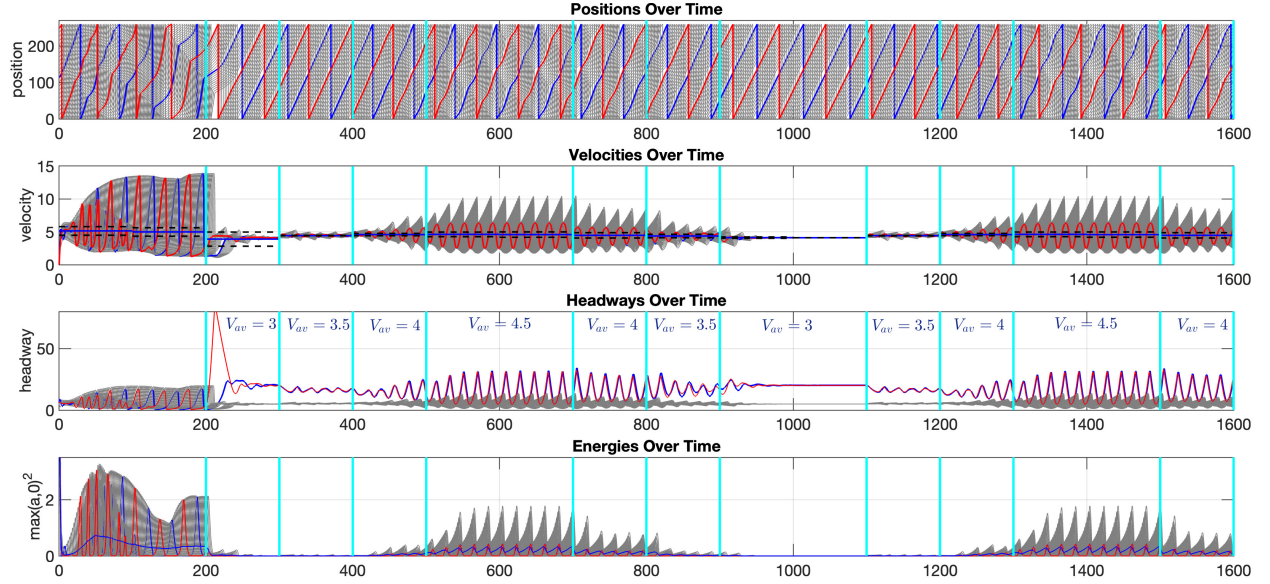


Figure 8: Case 3: Illustration of 21 HV + 2AV simulation. The red and blue curves plot the data for AV Car #23 and #11. Blue lines plot the mean velocity over each time intervals with length 100 and the average $\max(a, 0)^2$. The blue dotted curves plot the mean velocity \pm derivation.

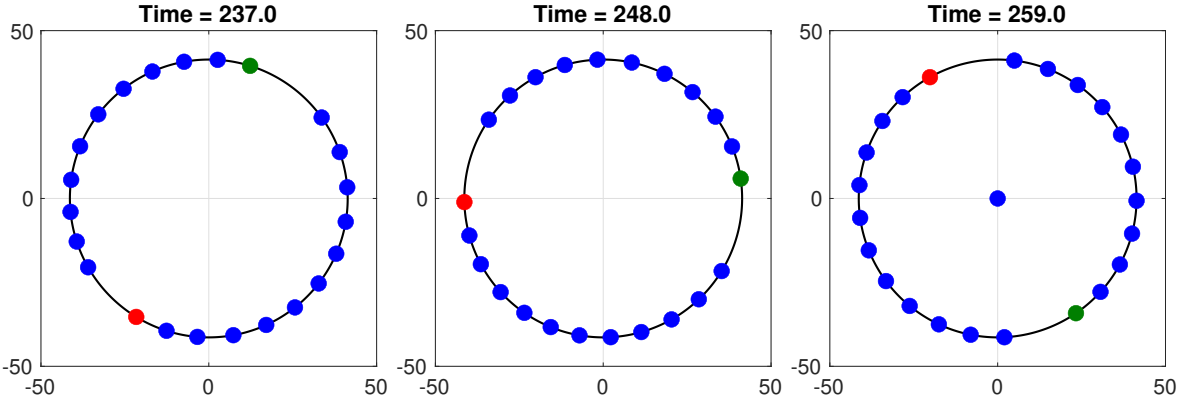


Figure 9: Case 3: Snapshot Plots

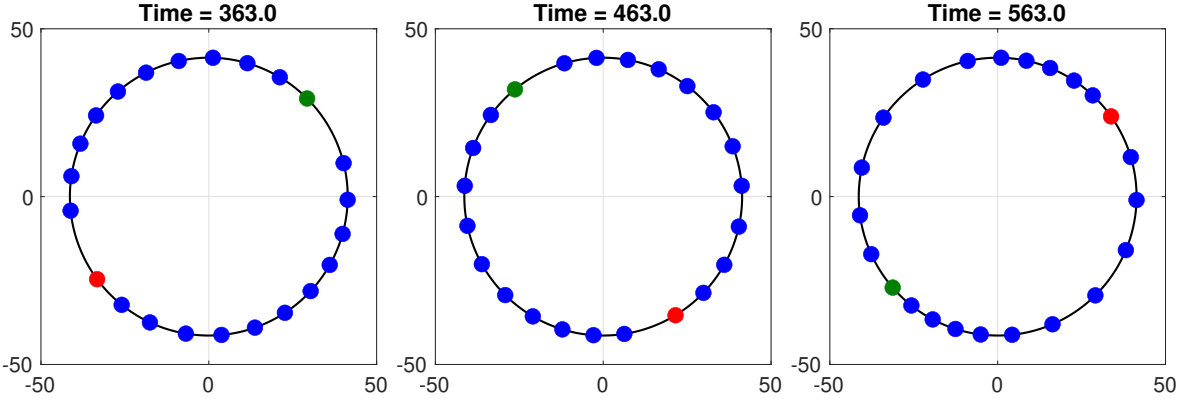


Figure 10: Case 3: Snapshot Plots

2.4. Summary of Numerical Observations

From Figures 3–8, it is evident that proper control of the AV(s) substantially modifies traffic flow patterns. Across all tested cases, controlled AVs dampen stop-and-go waves, reduce traffic instabilities, and lower energy expenditure. Quantitatively, the positive acceleration work, $\max(a, 0)^2$, which can serve as an indicator of fuel consumption, decreases as more AVs are introduced and appropriately controlled. These observations highlight the potential of optimal AV control to enhance traffic efficiency and reduce energy costs.

While the preliminary experiments (Cases 1–3) demonstrate these effects, it is important to note that we have not yet optimized numerical schemes or tuned control parameters such as $v_{\max,AV}$, α_{AV} , or β_{AV} ; these aspects are part of the proposed work. Overall, the results provide strong motivation for extending the framework to multi-class and hybrid ODE–PDE models to investigate broader traffic scenarios and systematically design optimal AV control strategies [3].

3. Conclusion and Outlook

These preliminary results confirm the potential of AV control to improve traffic efficiency and reduce fuel consumption. They provide a solid foundation for our proposed work on multi-class traffic models, numerical scheme development, and optimal control strategies. Future work will extend these simulations to hybrid models with heterogeneous traffic classes and explore optimized control laws for AVs.

References

- [1] F. van Wageningen-Kessels, H. van Lint, K. Vuik, and S. Hoogendoorn, "Genealogy of traffic flow models," *EURO Journal on Transportation and Logistics*, vol. 4, no. 4, pp. 445–473, 2015. doi: 10.1007/s13676-014-0045-5.
- [2] M. Bando, K. Hasebe, A. Nakayama, A. Shibata, and Y. Sugiyama, "Dynamical model of traffic congestion and numerical simulation," *Physical Review E*, 51(2):1035–1042, 1995.
- [3] R. E. Stern, S. Cui, M. L. Delle Monache, R. Bhadani, M. Bunting, M. Churchill, N. Hamilton, R. Haulcy, H. Pohlmann, F. Wu, B. Piccoli, B. Seibold, J. Sprinkle, and D. B. Work, "Dissipation of stop-and-go waves via control of autonomous vehicles: Field experiments," *Transportation Research Part C: Emerging Technologies*, 89:205–221, 2018.